actuators

MDPI

*Article*

# A Study on Eddy Current Reduction Shape of Single-Phase Claw-Pole Motor

**Na-Rim Jo[1], Ye-Seo Lee[1], Hyun-Jo Pyo[1], Dong-Hoon Jung[2], Kwang-Soo Kim[2] and Won-Ho @gaKim[3,*]**

[1] Department of Next Generation System Convergence, Gachon University, Seongnam 13120, South Korea; rimna9922@gmail.com (N-R.J.); yeseo9909@gmail.com (Y-S.L.); phj00700@naver.com (H-J.P.)
[2] School of Mechanical, Automotive and Robot Engineering, Halla University, Wonju 26404, Republic of Korea; dh.jung@halla.ac.kr (D-H.J.); kwangsoo2.kim@halla.ac.kr (K-S.K.)
[3] Department of Electrical Engineering, Gachon University, Seongnam 13120, Republic of Korea; wh15@gachon.ac.kr
* Correspondence: wh15@gachon.ac.kr

**Abstract:** The claw-pole motor, known for its simple structure, is widely used in various fields due to its cost competitiveness. However, a drawback of the fixed-stator type claw-pole motor is its vulnerability to eddy current losses. Therefore, this paper presents a single-phase claw-pole motor applied as a motor for cooling fans, with the aim of reducing eddy current losses and improving performance based on shape optimization, ultimately resulting in a single-phase claw-pole motor that meets the desired performance. The validity of this approach is verified through 3D finite element analysis (FEA).

**Keywords:** Claw-Pole; Single-Phase; Eddy Current Loss

## 1. Introduction

Considering recent fossil fuel depletion and energy regulations, the importance of energy conservation is becoming increasingly prominent. As a result, motor development has also been increasingly focused on high efficiency. High-performance rare-earth permanent magnets, which can enhance the performance of motors in terms of torque, output density, and efficiency, have emerged. This has led to active research in the field of permanent magnet synchronous motors [1]. However, due to rising material costs caused by inflation, an increase in the price of motors has become necessary. As a result, research efforts are actively underway worldwide to produce cost-competitive products by various companies. Because single-phase Drive ICs are more cost-competitive compared to three-phase Drive ICs, many motor applications in household appliances frequently utilize single-phase motors [2]. In pursuit of cost competitiveness, in addition to traditional radial flux motors, claw-pole motors, which employ ring-type permanent magnets, are being researched due to their simple and economical structure.

Motors that offer cost competitiveness often emphasize the importance of streamlining the manufacturing process and reducing material costs. Claw-pole motors, for instance, do not require laminated core plates and their straightforward structure simplifies the manufacturing process, making them suitable for cost savings [3-4]. Claw-pole motors are fundamentally shaped like claws, and their classification is based on the position of the "claw," leading to a basic categorization into rotor type and stator type, reflecting the attached name according to their core structure. In the case of the rotor type, it features a structure where the rotor contains coils or permanent magnets that are surrounded by the claws, resembling the shape of the claw enveloping them. On the other hand, the stator type replaces the traditional motor's shoes and teeth with the claws. In other words, the claw surrounds the stator coils in this structure. In this context, the advantage is that the

**Citation:** To be added by editorial staff during production.

Academic Editor: Firstname Lastname

Received: date
Revised: date
Accepted: date
Published: date

coils surrounded by the claw can utilize a ring-type winding configuration based on the shape characteristics of the claw. Especially, rotor-type claw-pole motors employ the slinky lamination method during stator production to maximize the utilization of electrical steel sheets. An advantage of these rotor-type claw-pole motors is that they can create multipole configurations based on the number of claws attached to the rotor, making them particularly suitable for use in automotive alternators. However, due to the rotor's winding, which includes brushes and a commutator, there is an inherent maintenance drawback. In contrast, stator-type claw-pole motors, utilizing permanent magnets in the rotor, offer a more cost-effective solution. Their compact and lightweight design is advantageous for various applications such as optical drives, hard disks, motor control in computer peripherals, drive motors, and more. Nevertheless, there is a disadvantage in that due to the structural characteristics of the claw and stator, laminated core plates cannot be used during their manufacturing, making them highly susceptible to eddy current losses. Therefore, this paper selects the single-phase stator-type claw-pole motor as the target application for cooling fan motors in microwave ovens and ovens, proposing a shape for reducing eddy current losses. This paper is divided into three main sections. In Section 1, the paper provides an explanation of the operating principles and manufacturing methods of the stator-type claw-pole motor. Section 2 describes the specifications of existing motors used in microwave ovens and ovens and discusses the characteristics of these motors when converted to stator-type claw-pole motors. Section 3 presents a formula for eddy current losses and proposes a shape for reducing eddy current losses through the analysis of the magnetic path and saturation in claw-pole motors. Furthermore, claw-pole motors have a shape that is not constant in the axial direction, unlike typical motors, and the magnetic paths generated in the rotor and stator of claw-pole motors occur in both radial and axial directions. Therefore, the validity of the proposed model was verified using 3D finite element analysis (FEA) [5].

## 2. Characteristics of single-phase stator claw-pole motor and driving principle

Figure 1 provides an explanation of the shape of the stator-type claw-pole motor. In (a), you can see the structure that includes the rotor, and in (b), the shape of the stator core is visible. As evident from the figure above, the rotor exhibits a shape similar to that of a surface permanent magnet synchronous motor (SPMSM) with permanent magnets attached to the back yoke. The stator core consists of components resembling claws and a stator back yoke, creating a slotted structure. Within these slots, there is a ring-type winding, and the number of stacked stator cores determines the phase count, resembling a configuration where cans are stacked, hence the term "can stack motor." In this paper, as it is based on single-phase motors, there is only one stator, as shown in (b).

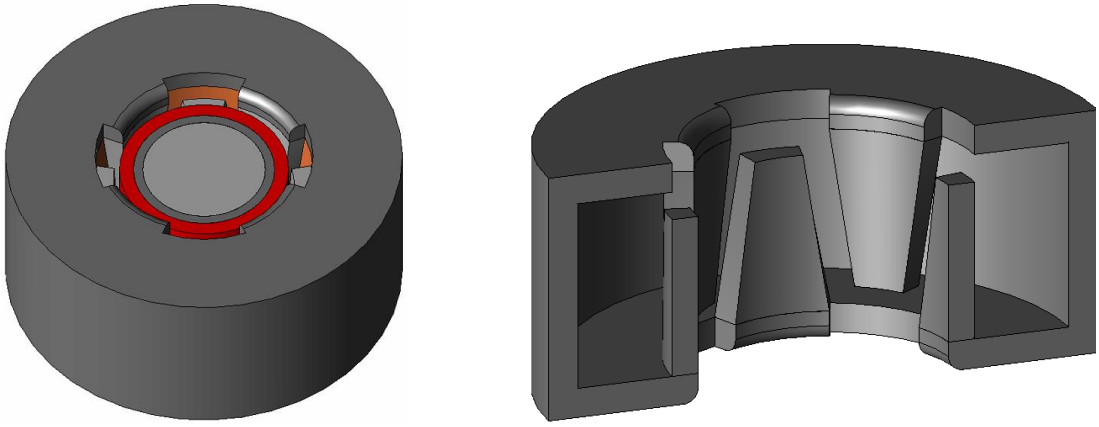

(**a**) (**b**)

**Figure 1.** Shape of the single-phase stator-type claw-pole motor: (a) Overall shape; (b) Stator core shape.

The structure of the stator is notably different from the typical core-type motor, and because of these characteristics, laminated core plates cannot be used. In the manufacturing of Claw-Pole motor stators, the deep drawing method is employed. Deep drawing is a process that essentially involves pressing a punch onto the sheet metal surface to shape it according to the mold's form. The process of deep drawing is categorized as “deep” if the depths of pressing reachs a diameter of part is to be formed[6-7]. Due to this manufacturing process, laminated core plates cannot be used for the stator core. Instead, a material with excellent machinability and formability is required, which is why steel plate cold commercial (SPCC), a type of cold-rolled steel product, is chosen as the material for the stator core. Figure 2 illustrates the stator manufacturing process of a claw-pole motor using the deep drawing method. A part of the stator core is bent and extended using a punch to create the claw shape. However, SPCC is a material that is susceptible to magnetic saturation due to its lower permeability and saturation level compared to electrical steel sheets.

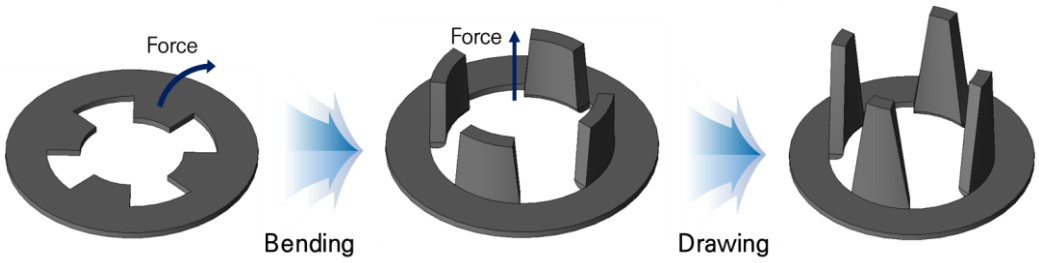


**Figure 2.** The concept of manufacturing the claw using deep drawing processing.

The operating principle of the single-phase claw-pole motor, as shown in Figure 3, is determined by the direction of the current in the armature winding. This direction of current results in the generation of magnetic paths in the claw, either above or below, thereby determining the polarity. The interaction between the magnetic field generated in the claw and the permanent magnets results in the generation of a force that drives the rotation in one direction due to attraction and repulsion forces. In this situation, two different cases of magnetic paths occur. One case is when there is only one pole of permanent magnets on the claw, and the other case is when the claw has permanent magnets with different poles. When there is only one pole of permanent magnets on the claw, the magnetic path is as follows: Permanent Magnet (N) - Claw (N) - Stator Yoke - Claw (S) - Permanent Magnet (S). The magnetic flux entering from the permanent magnet's south pole exits through the internal path to the permanent magnet's north pole. When the rotor has moved by half a pitch, and there are permanent magnets with opposite poles on the claw, the magnetic path follows this route: Permanent Magnet (N) - Claw (N) - Permanent Magnet (S) [8-12]. In this case, it's evident that the magnetic path has a shorter route compared to when one pole of a permanent magnet faces the claw. As a result, due to the ever-changing magnetic path based on the rotor's position in the claw-pole motor, fluctuations in magnetic stored energy occur. These differences in magnetic stored energy drive the operation of the claw-pole motor.

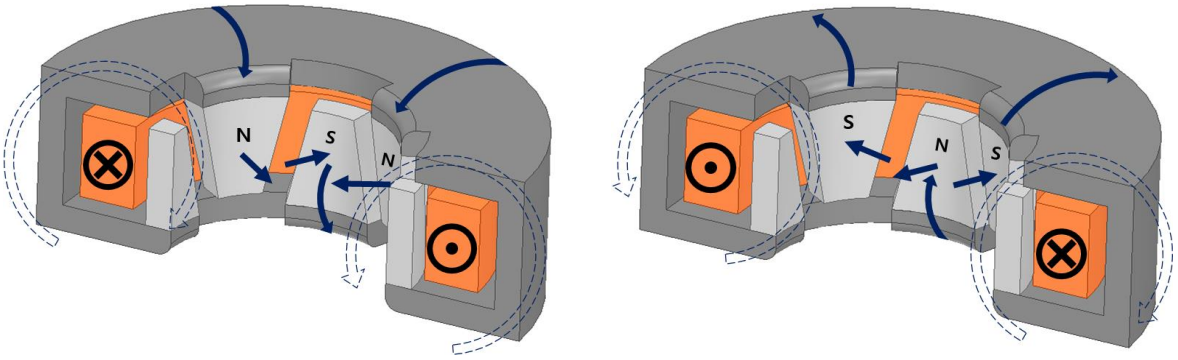


(**a**) (**b**)

**Figure 3.** Claw polarity and magnetic field direction in a stator-type claw-pole motor based on the current direction: (a) Clockwise current input; (b) Counterclockwise current input.

## 3. Basic design of single-phase stator type claw-pole motor

To undertake the basic design of a single-phase claw-pole motor, it is essential to examine the shape and specifications of an existing cooling fan motor, as shown in Figure 4. Figure 4 (a) represents the mass-produced model of the existing cooling fan motor, while (b) is the 3-phase model developed for cost savings. In the case of conventional induction motors, the difficulty in speed control led to the use of 11 different motors, resulting in disadvantages for maintenance and upkeep. As a solution, research has been conducted to transition to permanent magnet (PM) motors. Hence, considering the size constraints, the stator stack height remains the same as the conventional induction motor at 15mm, and the outer diameter is 39mm, taking the shaft into account. The target output power is also identical to the existing cooling fan motor, which is 5.5W. In this case, the target motor is based on a 3-phase SPMSM (Surface Permanent Magnet Synchronous Motor), and the goal is to adapt it into a single-phase claw-pole motor.

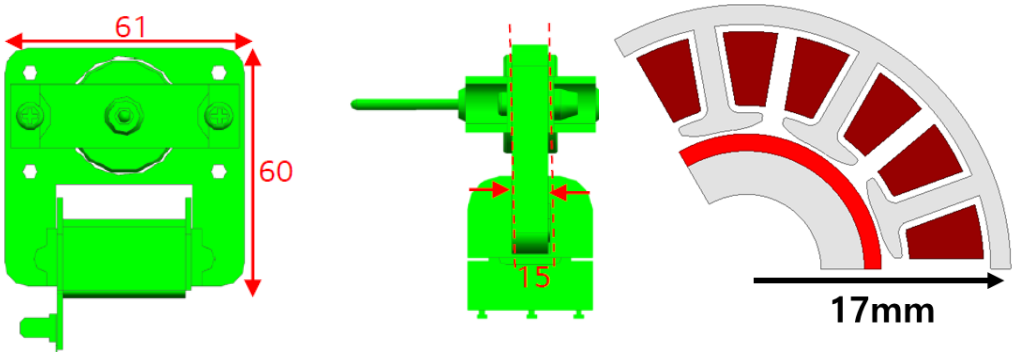


(a) (b)

**Figure 4.** Existing cooling fan motor shape and size specifications: (a) Single-phase induction motor shape; (b) 3-phase motor shape.

To select the number of poles for the single-phase claw-pole motor, a comparative analysis is carried out for unloaded eddy current losses and back electromotive force (EMF) from 4 poles to 10 poles. For the single-phase claw-pole motor, considering a 1:1 ratio between the poles of permanent magnets and claws, the comparative analysis starts from 4 poles. It is important to consider that motors with more than 12 poles at the current size face manufacturing challenges, so a comparison of back electromotive force (EMF) is carried out up to 10 poles under unloaded conditions. in this case, the back electromotive force (EMF) increases up to 10 poles, which is advantageous for performance. However, it is essential to note that the eddy current losses also increase. Based on the results in

Figures 5 and 6, models with 8 poles or fewer are selected to balance performance and eddy current losses.

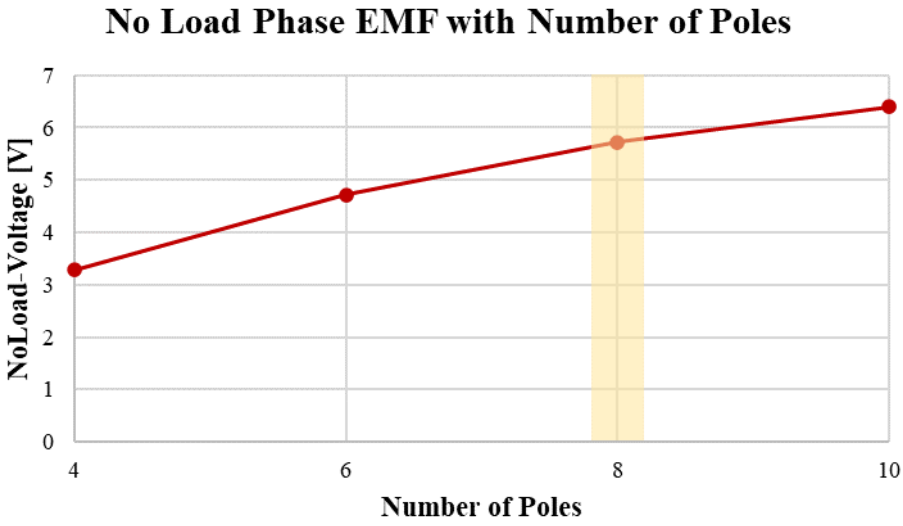


**Figure 5.** Comparative analysis of back electromotive force (EMF) for different numbers of poles under unloaded conditions.

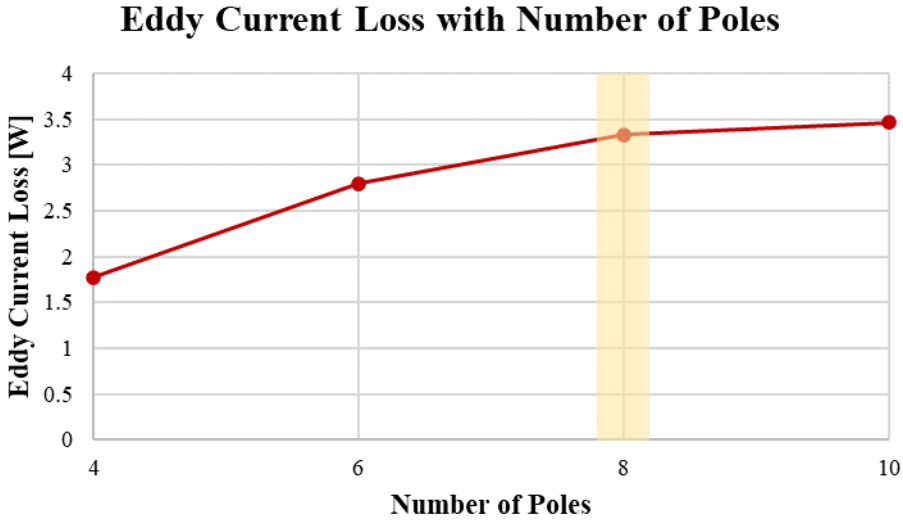


**Figure 6.** Comparative analysis of eddy current losses for different numbers of poles.

For motors with non-laminated cores, the loss characteristics vary significantly depending on the core's structure and thickness. Therefore, it's important to consider the eddy current losses calculated based on the stacking factor. Due to the significant analysis time required, when conducting trend analysis, it's common to not consider eddy current losses and asymmetric core structures. The basic design of the single-phase claw-pole motor, which fits within the size constraints of the existing motor, is shown in Figure 7, and the performance is presented in Table 2.

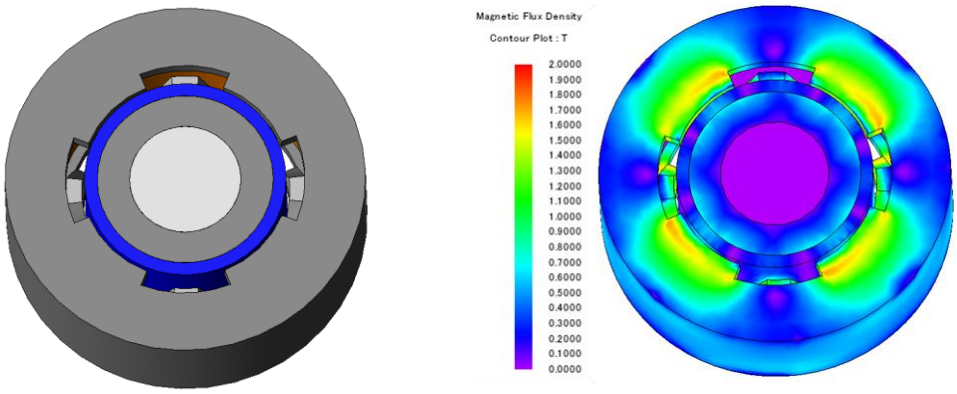


(a) (b)

**Figure 7.** Identical size model to the existing 3-phase cooling fan motor: (a) Shape; (b) Magnetic flux density.

**Table 1.** Performance of the existing 3-phase cooling fan motor.

| Parameter | Value | Unit |
|---|---|---|
| Power | 3.63 | W |
| Speed | 2950 | rpm |
| Torque | 12.38 | mNm |
| Current | 0.486 | Arms |
| Current density | 7.96 | Arms/mm$^2$ |
| Voltage | 13.57 | V |
| Number of turns | 129 | - |

When the motor is the same size as the existing model, it doesn't meet the target torque of 18 [mNm]. Therefore, a design is needed to increase the total magnetic loading and total electric loading for torque enhancement. The equation related to total magnetic loading is the same as Equation 1, and the equation related to total electric loading is expressed in Equation 2.

$$Total\ magnetic\ loading = 2p\phi_g\ [T] \quad (1)$$

$$Total\ electric\ loading = I_a Z\ [Ampere\ Conductor] \quad (2)$$

In Equation 1, $p$ represents the pole pair number, $\phi_g$ denotes the average gap flux per pole, and in Equation 2, $I_a$ represents phase current, while $Z$ represents the total number of conductors in the stator. As can be seen from the equations, increasing the electrical and magnetic loadings requires an increase in size. Therefore, an analysis of performance characteristics in relation to the increase in stack length and outer diameter is conducted. The shape characteristics are analyzed by adjusting the stack length and outer diameter based on the same volume and magnet usage to design a single-phase claw-pole motor that meets the target performance. Figure 8 shows the shapes and magnetic saturation densities of each model, with the extent of size increase expressed as a percentage. Model (a) in Figure 8 increased the stack length by 2.3mm, and model (b) increased the outer diameter by 3.32mm compared to the base model.

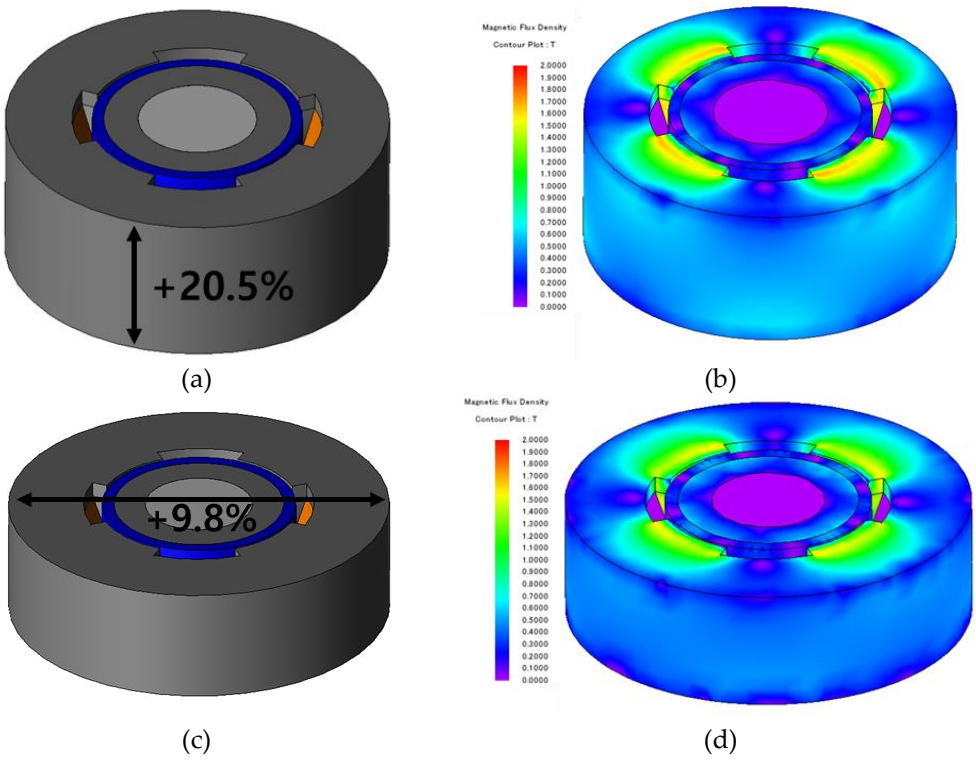


**Figure 8**. Model with increased stack length and outer diameter: (a) Model with increased stack length shape; (b) Model with increased stack length magnetic saturation density; (c) Model with increased outer diameter shape; (d) Model with increased outer diameter magnetic saturation density.

**Table 2.** Performance comparison of the increased stack length model and increased outer diameter model.

| Parameter | Value | | Unit |
|---|---|---|---|
| Model | Increased stack length | Increased outer diameter | - |
| Power | 5.55 | 5.5 | W |
| Speed | 2950 | 2950 | rpm |
| Torque | 18.6 | 18.43 | mNm |
| Current | 0.486 | 0.486 | Arms |
| Current density | 7.96 | 7.96 | Arms/mm$^2$ |
| Voltage | 21.53 | 22.02 | V |
| Number of turns | 182 | 197 | - |

Increasing the stack length and outer diameter resulted in an increase in the slot cross-sectional area, and, with a constant slot fill factor, the number of turns also increased. While the model with increased stack length had 15 more turns compared to the model with increased outer diameter, the increased stack length also led to an increase in the effective cross-sectional area for generating torque, resulting in an overall torque increase. Therefore, the design will proceed based on the model with increased stack length. In the case of the single-phase claw-pole motor, there are performance losses due to eddy current losses and uneven air gap, so the analysis will be carried out with performance margins taken into account, considering the maximum stack length within the same volume and then analyzing the eddy current losses. Figure 9 shows the shape and magnetic flux density distribution of the single-phase claw-pole motor with the same stack length as the conventional induction motor. Table 3 displays the performance of the model with the maximum stack length.

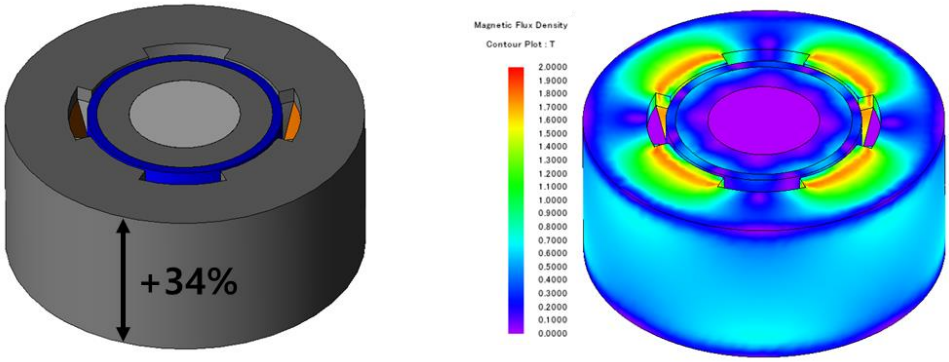


(a) (b)

**Figure 9.** Shape and magnetic flux saturation density of the maximum stacking length model: (a) stacking length maximum model shape; (b) stacking length maximum model flux saturation density.

**Table 3.** Performance of a single-phase claw-pole motor with maximum stacking length.

| Parameter | Value | Unit |
|---|---|---|
| Model | Maximum stacking length | - |
| Power | 1.79 | W |
| Speed | 2950 | rpm |
| Torque | 5.81 | mNm |
| Current | 0.486 | Arms |
| Current density | 7.96 | Arms/mm$^2$ |
| Voltage | 20.54 | V |
| Number of turns | 216 | - |
| Claw eddy current loss | 1.35 | W |
| Stator back yoke eddy current loss | 2.41 | W |

The model with the maximum stack length does not meet the target performance when considering the eddy current loss. To achieve the desired performance, it is necessary to design for an increase in the field strength. The sum of the magnetic flux from permanent magnets and the demagnetizing effect caused by the stator current generates the eddy current. To reduce the no-load saturation, electrical loading is maximized to consider the eddy current loss. To maximize the electrical loading, the magnet thickness and the rotor back yoke thickness are minimized. To improve the magnetic flux density, the stator back yoke thickness is increased from the existing 1.5mm to 1.8mm. Performance comparisons and analyses are conducted for models with up to 8 poles.

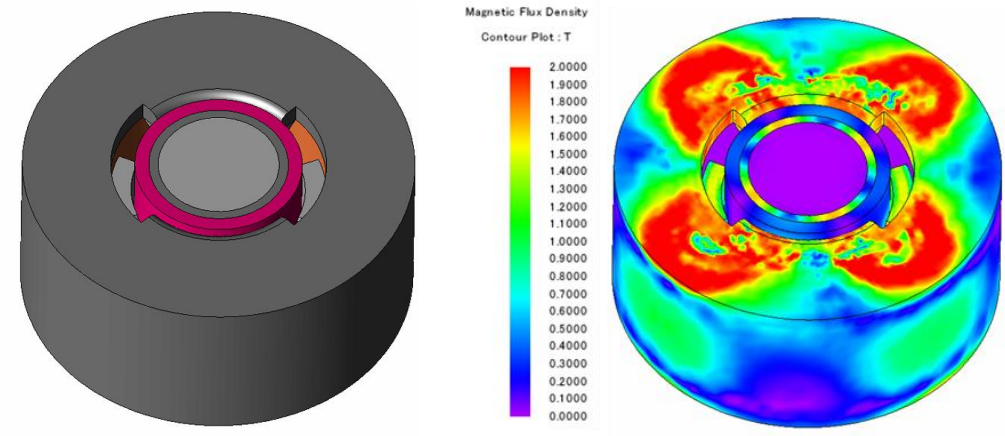


(a) (b)

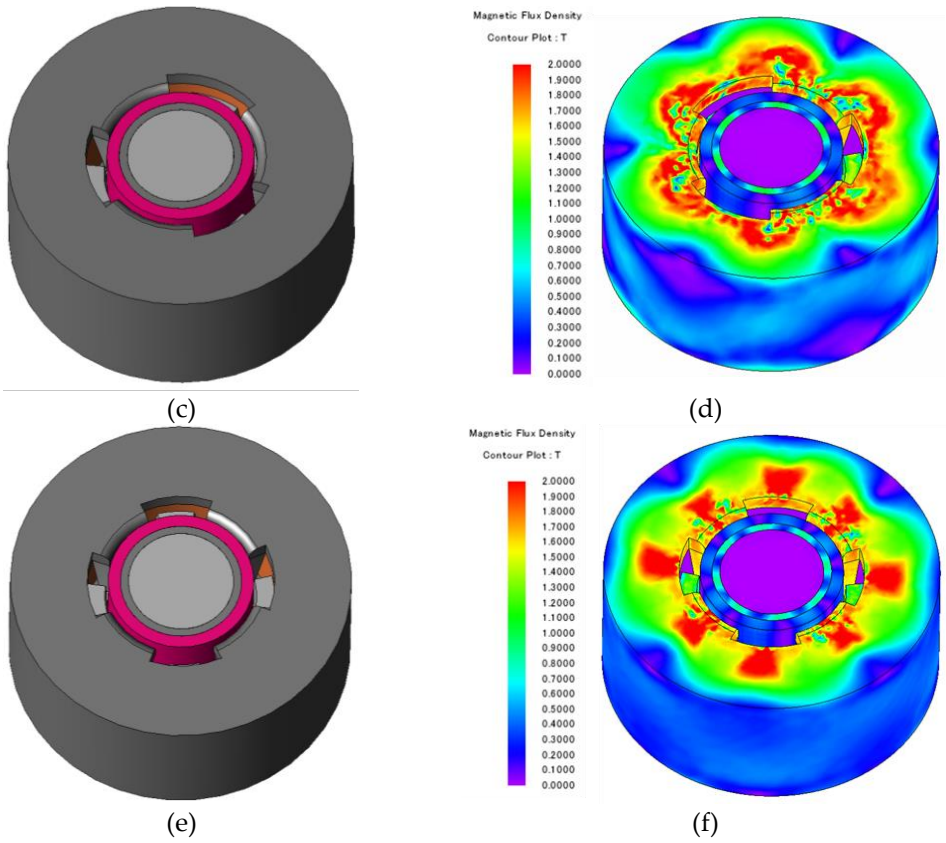


**Figure 10.** Shape and magnetic flux saturation density of a single-phase claw-pole motor: (a) 4-pole shape; (b) magnetic flux saturation density of 4-pole model; (c) 6-pole shape; (d) magnetic flux saturation density of 6-pole model; (e) 8-pole shape; (f) magnetic flux saturation density of 8-pole model.

**Table 4.** Performance comparison of single-Stage claw-pole motor by pole numbers.

| Parameter | Value | | | Unit |
|---|---|---|---|---|
| Model | 4 Poles | 6 Poles | 8 Poles | - |
| Power | 3.32 | 4.6 | 5.72 | W |
| Speed | 2950 | 2950 | 2950 | rpm |
| Torque | 10.74 | 14.89 | 18.52 | mNm |
| Current | 0.486 | 0.486 | 0.486 | $A_{rms}$ |
| Current density | 7.96 | 7.96 | 7.96 | $A_{rms}/mm^2$ |
| Voltage | 23.79 | 31.57 | 38.05 | V |
| Number of turns | 398 | 398 | 398 | - |
| Claw eddy current loss | 0.82 | 1.1 | 1.31 | W |
| Stator back yoke eddy current loss | 1.62 | 2.12 | 2.7 | W |

In Table 4, comparing the 4 poles with the least loss and the 8 poles with the most loss, it can be seen that the eddy current loss increases by 64.3%. However, in the single-phase claw-pole motor of this paper, the claw occupies half of the pole pitch below and the upper part as much as the pole pitch, so the smaller the number of poles, the smaller the length of the physical claw. As the number of poles increases, the torque also increases, but once the number of poles exceeds a certain point, the extent of leakage between the poles increases, leading to a decrease in torque. Therefore, based on the table, we can observe that the torque increases by 72.4% when comparing the 4-pole configuration. Considering the target performance and performance reduction due to the asymmetric structure of the air gap, the 8-pole model appears to be the most suitable choice. Therefore, we select the 8-pole model to reduce eddy current losses.

## 4. Reduction of eddy current loss in single-phase stator type Claw-Pole motor design

### *4.1. Reduction of eddy current loss based on the rotor under-hang model.*

Most single-phase claw-pole motors, as seen in Figure 11, exhibit a magnetic flux path where magnetic resistance is relatively low, mainly occurring in the claw and the adjacent stator back yoke.

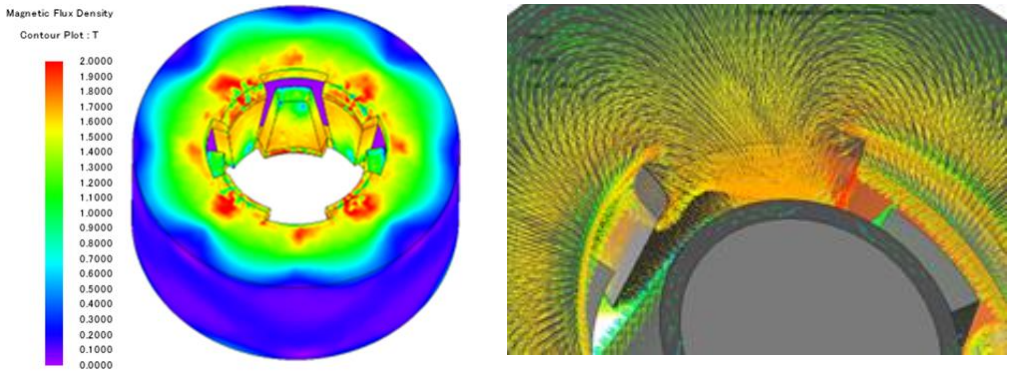


(a) (b)

**Figure 11.** Saturation density and magnetic path in the single-phase claw-pole motor stator: (a) stator saturation flux density; (b) magnetic path.

In other words, most of the eddy current losses are directly affected by changes in magnetic flux over time, occurring primarily in the lower portion of the claw with relatively low magnetic resistance and in the stator yoke adjacent to the claw. When considering the reduction of eddy current losses in the single-phase claw-pole motor model, the formula for reducing eddy current losses is similar to Equation 3.

$$P_e = K_e B_{max}^2 f^2 t^2 V \ [W] \tag{3}$$

In Equation 3, $P_e$ represents eddy current loss, $K_e$ is the eddy current factor, $B_{max}$ denotes the maximum magnetic flux density, $f$ tands for frequency, $t$ indicates material thickness, and $V$ represents volume. To reduce eddy current losses, the physical length of the rotor's permanent magnets is reduced to decrease the values of t and V in Equation 3. An under-hang structure is implemented to reduce the rotor's lamination length by the thickness of the stator back yoke, as illustrated in Figure 12, and the performance specifications are provided in Table 6.

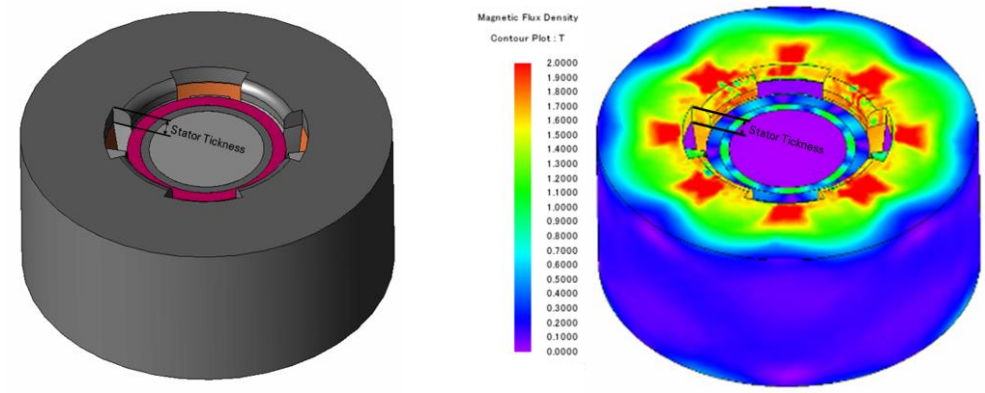


(a) (b)

**Figure 12.** The model shape and magnetic flux saturation density of the rotor under-hang application: (a) rotor under-hang model shape; (b) rotor under-hang model magnetic flux saturation density.

**Table 5.** Specifications of the rotor under-hang application model performance.

| Parameter | Value | Unit |
|---|---|---|
| Model | Rotor under-hang application | - |
| Power | 5.61 | W |
| Speed | 2950 | rpm |
| Torque | 18.2 | mNm |
| Current | 0.486 | Arms |
| Current density | 7.96 | Arms/mm$^2$ |
| Voltage | 37.66 | V |
| Number of turns | 398 | - |
| Claw eddy current loss | 1.3 | W |
| Stator back yoke eddy current loss | 2.49 | W |

When the rotor under-hang structure was applied, the torque decreased by 1.73% compared to the conventional 8-pole model. However, it was found that total core loss can be reduced by 5.49%. Therefore, using this model as a reference, an asymmetrical air gap structure is applied to shift the cogging torque phase and secure the starting torque. A single-phase motor, unlike a three-phase motor, utilizes a squirrel cage rotor. In the case of a single-phase PM BLDC motor with a uniform air gap, a dead zone occurs where the zero torque positions of the pull-in torque and cogging torque coincide, rendering it essentially incapable of self-starting.[13-16]. Therefore, an asymmetric air gap shape is applied to shift the zero-point position of the cogging torque and the zero-point torque, allowing for self-starting. To meet voltage limitations, the wire density is increased based on the same current density criterion. The shape and torque phase shift of the single-phase claw-pole motor with an asymmetric air gap structure are depicted in Figure 13, and the performance specifications are presented in Table 6.

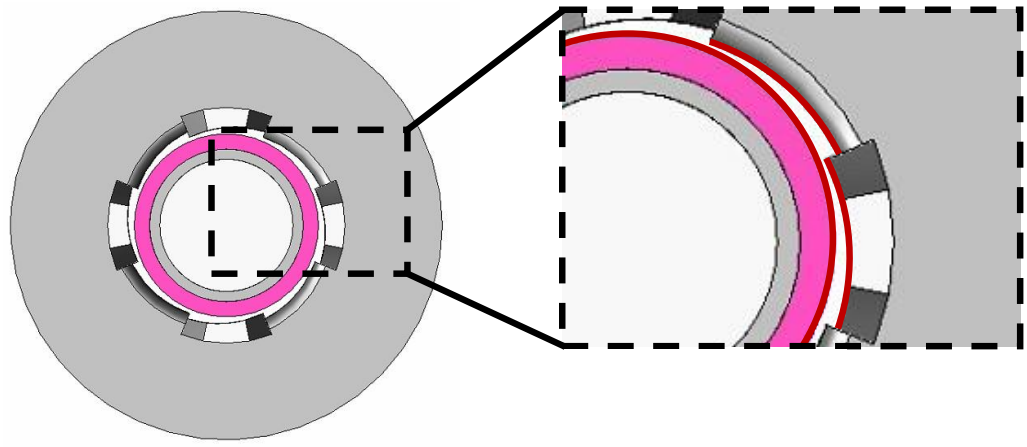

(a)

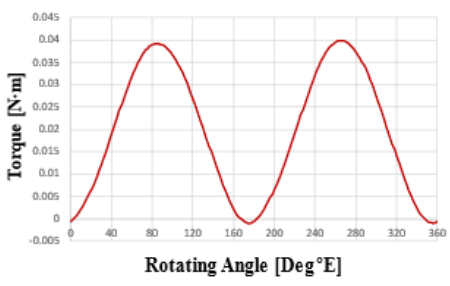


(b)

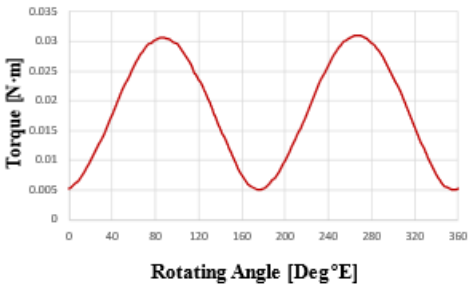


(c)

**Figure 13.** Asymmetrical air gap structure applied configuration and torque waveforms: (a) Asymmetrical air gap structure shape; (b) Conventional torque waveform; (c) Torque waveform when the asymmetrical air gap structure is applied.

**Table 6.** Performance specifications of the asymmetrical air gap applied model.

| Parameter | Value | Unit |
|---|---|---|
| Model | Asymmetrical air gap application | - |
| Power | 5.32 | W |
| Speed | 2950 | rpm |
| Torque | 17.21 | mNm |
| Current | 1.76 | Arms |
| Current density | 7.96 | $A_{rms}/mm^2$ |
| Voltage | 9.33 | V |
| Number of turns | 110 | - |
| Claw eddy current loss | 0.86 | W |
| Stator back yoke eddy current loss | 1.71 | W |

*4.2. Reduction of eddy current losses based on slit structure.*

Through equation 3, it can be observed that eddy current losses are proportional to the square of the conductor thickness. To reduce eddy current losses, we consider the saturation and magnetic path of the single-phase claw-pole motor. As shown in Figure 14, we insert air insulation into the stator core and reduce the conductor thickness. The eddy current path of the single-phase claw-pole motor is illustrated in Figure 15, showing the application of two air insulations to reduce the conductor thickness to 1/3.

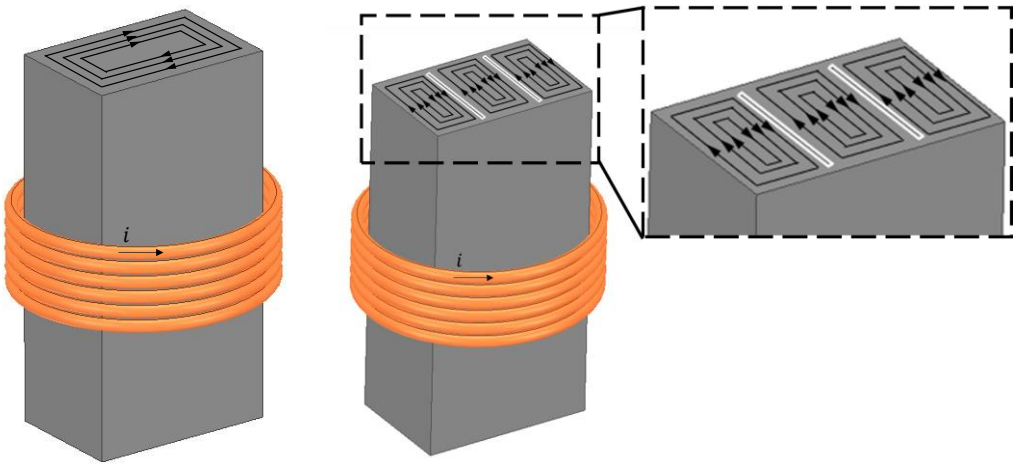


(a) (b)

**Figure 14.** Conceptual diagram of air insulation application: (a) without air insulation; (b) with air insulation.

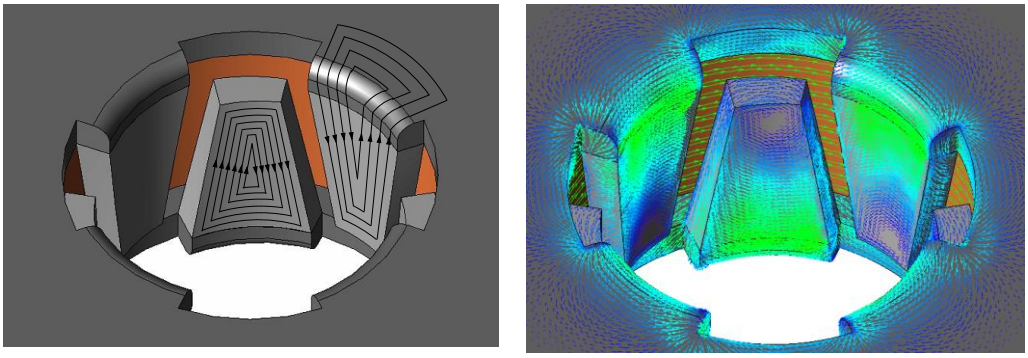

**Figure 15.** Eddy current path in the single-phase claw-pole motor.

When applying air insulation and the slit structure, it is essential to consider not interfering with the magnetic path of the stator and account for the core's saturation. In the claw-pole motor, the eddy current path, as described in Figure 15, is directly influenced by the time rate of change of the magnetic field and is relatively larger in cross-sectional area, resulting in the highest magnetic resistance in the claw, stator back yoke, and stator areas between the claws. Therefore, identical length and thickness slit structures are applied to these regions. Based on the location of the applied slits for air insulation, different shapes of the single-phase claw-pole motor are proposed, and the eddy current characteristics are examined. Four types of slits, labeled as slit 1, 2, 3, and 4, are compared depending on their application positions. Slit 1 is applied to the claw, slit 2 to the stator yoke adjacent to the claw, slit 3 to the stator between the claws, and slit 4 combines the most effective slit, slit 1, and slit 3 to reduce eddy current losses. By inserting air insulation, it generates the time rate of change of the magnetic field, which is the source of eddy current. This results in an increase in electrical resistance per unit area, leading to a reduction in eddy current losses. As a result, the stator core can be effectively stacked similar to a conventional radial flux PM motor, and the saturation is depicted in Figure 16.

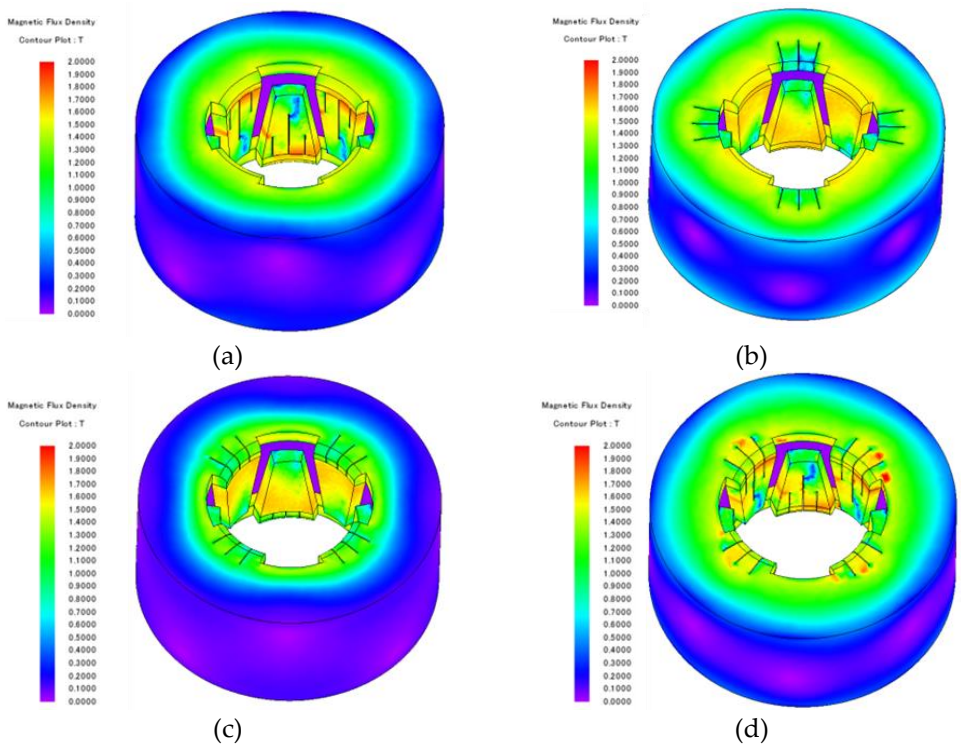


**Figure 16.** Magnetic saturation of the single-phase claw-pole motor with air insulation applied in different locations: (a) Slit 1; (b) Slit 2; (c) Slit 3; (d) Slit 4.

**Table 7.** Performance specifications based on the air insulation location in the single-phase claw-pole motor.

| **Parameter** | **Value** | | | | **Unit** |
|---|---|---|---|---|---|
| Model | Slit 1 | Slit 2 | Slit 3 | Slit 4 | - |
| Power | 5.41 | 5.45 | 5.56 | 5.51 | W |
| Speed | 2950 | 2950 | 2950 | 2950 | rpm |
| Torque | 17.53 | 17.63 | 17.99 | 17.83 | mNm |
| Current | 1.76 | 1.76 | 1.76 | 1.76 | Arms |
| Current density | 7.96 | 7.96 | 7.96 | 7.96 | $A_{rms}/mm^2$ |
| Voltage | 9.54 | 9.41 | 9.5 | 9.44 | V |

| | | | | | |
|---|---|---|---|---|---|
| Number of turns | 110 | 110 | 110 | 110 | - |
| Claw eddy current loss | 0.71 | 0.84 | 0.86 | 0.68 | W |
| Stator back yoke eddy current loss | 1.83 | 1.56 | 1.3 | 1.7 | W |

Through Table 7, it can be observed that eddy current losses are reduced based on the location of air insulation, resulting in an increase in torque. In the case of the claw-pole model, the performance decrease due to eddy current losses is significant, so it is evident that performance increases when eddy current losses are reduced. Comparing the Slit 1, 2, 3, 4 models to the models with asymmetrical air gaps and under-hang application in Table 7, each of them shows a reduction in eddy current losses by 1.17%, 6.61%, 15.95%, and 7.39%, respectively, with an increase in torque by 1.88%, 2.44%, 4.53%, and 3.63%, as illustrated in Figure 17.

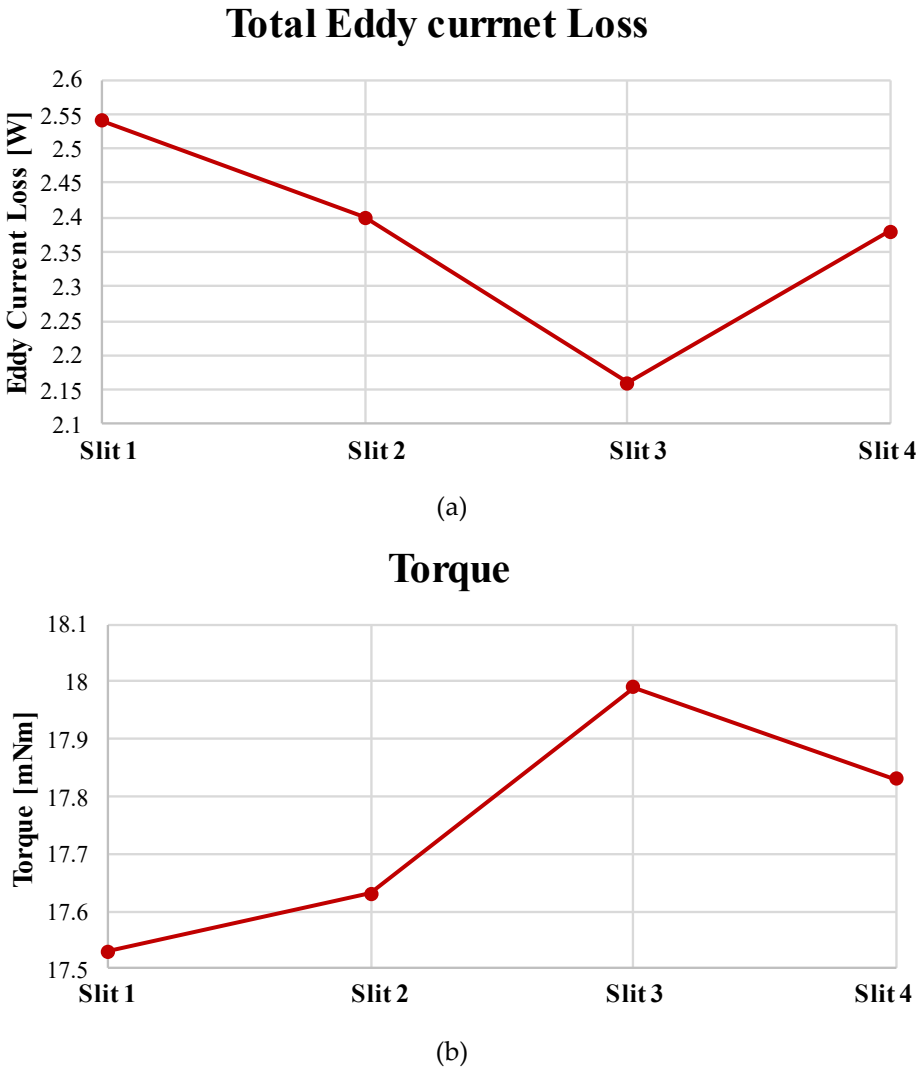


**Figure 17.** Performance analysis based on the Slit models: (a) Eddy current loss comparison; (b) Torque comparison.

In the case of Slit 4, even though it combines two of the most effective Slit models, the increase in the number of air insulations leads to an increase in stator saturation due to the reduction in cross-sectional area of the magnetic path. As a result, it's evident that eddy current losses increase compared to the Slit 3 model. Therefore, when applying air insulation, it is essential to consider the magnetic path and saturation. Furthermore, when

comparing the eddy current losses of the 8-pole model from Table 4 with the most effective Slit 3 model in reducing eddy current losses, it is confirmed that the Slit 3 model reduces eddy current losses by 46.15%. This has resulted in the derivation of a model that satisfies the target output of 5.5W based on 3D FEA.

## 5. Conclusions

This paper conducted a study to convert a three-phase cooling fan motor into a single-phase claw-pole motor, while adhering to the size constraints of the existing stator. To address the challenge of maintenance and servicing difficulties associated with the induction motor, it was replaced with a three-phase BLDC motor. However, although a three-phase BLDC motor was chosen as the target motor, it was found that a single-phase stator claw-pole motor is particularly vulnerable to eddy current losses, which prevented it from meeting the performance requirements within the same size constraints. As a result, it was necessary to develop a design that increases efficiency in order to enhance performance. The study included an analysis of the performance characteristics concerning the size of the claw-pole motor. The analysis of performance characteristics concerning size concluded that increasing the stack length can increase the effective cross-sectional area for generating torque. To reduce eddy current losses, the design aimed to maximize the electrical stack length. Additionally, by comparing performance characteristics based on the number of poles, a fundamental model was designed, taking into consideration the pole count. Most of the eddy current losses are directly affected by the rate of change of magnetic field within the magnetic path. They primarily occur in the lower section of the claw and in the stator yoke adjacent to the claw, where magnetic resistance is relatively low. To address this, the rotor under-hang structure was applied. It resulted in a 5.49% reduction in eddy current losses compared to the 1.73% reduction in torque, which is considered a reasonable outcome. To further reduce eddy current losses, air insulation was inserted. In the case of the Slit 4 model, even though it combines the Slit 1 and Slit 3 models, an increase in the number of slits led to an increase in stator saturation due to the reduction in the cross-sectional area of the magnetic path. Consequently, eddy current losses increased. Therefore, the Slit 3 model, when compared to the state before inserting air insulation, showed a 4.53% increase in torque and a 15.95% reduction in eddy current losses, making it the most effective in reducing eddy current losses. A model that meets the performance requirements was derived and validated for feasibility through 3D FEA.

**Author Contributions:** Conceptualization, W.-H.K.; methodology, N.-R.J.; software, Y.-S.L.; validation, N.-R.J.; formal analysis, Y.-S.L.; investigation, H.-J.P.; resources, N.-R.J.; data curation, K.-S.K.; writing—original draft preparation, N.-R.J.; writing—review and editing, H.-J.P. and D.-H.J.; visualization, K.-S.K. and D.-H.J.; supervision, W.-H.K. All authors have read and agreed to the published version of the manuscript.

**Funding:** Please add: This research was funded by Department of Next Generation Energy System Convergence based-on Techno-Economics—STEP) and in part by This work was supported by the Gachon University research fund of 2021, Basic Science Research Program through the National Research Foundation of Korea (NRF) funded by the Ministry of Education (No. NRF-2022R1I1A3068863).

**Data Availability Statement:** Not applicable.

**Conflicts of Interest:** The authors declare no conflict of interest.

## References

1. M. A. Rahman and T. A. Little, "Dynamic Performance Analysis of Permanet Magnet Synchronous Motors Magnet Synchronous Motors," in IEEE Transactions on Power Apparatus and Systems, vol. PAS-103, no. 6, pp. 1277-1282, June 1984, doi: 10.1109/TPAS.1984.318460.

2. Lee, J.-H.; Jung, S.-Y. Noise Reduction Design with Trapezoidal Back-EMF and Asymmetric Air-Gap for Single-Phase BLDC Refrigerator Cooling Fan Motor. Energies 2021, 14, 5467. https://doi.org/10.3390/en14175467
3. Zhang, Y.; Gao, M.; Wang, L.; Zhang, X.; Xu, M.; Hu, W.; Wang, L. Study of Electromagnetic Characteristics of Brushless Reverse Claw-Pole Electrically Excited Generators for Automobiles. Energies 2023, 16, 2573. https://doi.org/10.3390/en16062573
4. S. -B. Lim, D. -S. Jung, K. -C. Kim, D. -H. Koo and J. Lee, "Characteristic Analysis of Permanent-Magnet-Type Stepping Motor With Claw Poles by Using 3 Dimensional Finite Element Method," in IEEE Transactions on Magnetics, vol. 43, no. 6, pp. 2519-2521, June 2007, doi: 10.1109/TMAG.2007.893999.
5. Dae-Sung Jung, Seung-Bin Lim, Sung Gu Lee and Ju Lee, "A study on the improvement of static characteristic in claw poled permanent magnet stepping motor," 2006 12th Biennial IEEE Conference on Electromagnetic Field Computation, Miami, FL, USA, 2006, pp. 120-120, doi: 10.1109/CEFC-06.2006.1632912.
6. Y. Y. Martawirya, S. Raharno and D. Sadono, "Preliminary study of a deep drawing process modelling for AL-5083 aluminium material," 2014 International Conference on Electrical Engineering and Computer Science (ICEECS), Kuta, Bali, Indonesia, 2014, pp. 315-320, doi: 10.1109/ICEECS.2014.7045269.
7. S. Shi, "The Research of Feedback-Feedforward Iterative Learning Control in Hydrodynamic Deep Drawing Process," 2015 14th International Symposium on Distributed Computing and Applications for Business Engineering and Science (DCABES), Guiyang, China, 2015, pp. 423-426, doi: 10.1109/DCABES.2015.112.
8. A. Ibala and A. Masmoudi, "3D FEA based feature investigation of a claw pole alternator with DC excitation in the stator," 2010 7th International Multi- Conference on Systems, Signals and Devices, Amman, Jordan, 2010, pp. 1-6, doi: 10.1109/SSD.2010.5585533.
9. S. Leitner, T. Kulterer, H. Gruebler and A. Muetze, "Characterization of the Thermal Performances of Low-Cost Sub-Fractional Horsepower BLDC Claw-Pole Motor Designs," 2020 IEEE Energy Conversion Congress and Exposition (ECCE), Detroit, MI, USA, 2020, pp. 4269-4275, doi: 10.1109/ECCE44975.2020.9236284.
10. Y. Dong, X. Li, X. Wang, K. Lu and X. Feng, "Design and Analysis of Electric-Excitation Claw-Pole Field-Modulated Machine Considering Effective Harmonics," 2022 IEEE Energy Conversion Congress and Exposition (ECCE), Detroit, MI, USA, 2022, pp. 1-6, doi: 10.1109/ECCE50734.2022.9948124.
11. D. Elloumi, A. Ibala, R. Rebhi and A. Masmoudi, "Lumped Circuit Accounting for the Rotor Motion Dedicated to the Investigation of the Time-Varying Features of Claw Pole Topologies," in IEEE Transactions on Magnetics, vol. 51, no. 5, pp. 1-8, May 2015, Art no. 8105108, doi: 10.1109/TMAG.2015.2405896.
12. W. Zhang, Y. Xu and M. Sun, "Design of a Novel Claw Pole Transverse Flux Permanent Magnet Motor Based on Hybrid Stator Core," in IEEE Transactions on Magnetics, vol. 57, no. 6, pp. 1-5, June 2021, Art no. 8104705, doi: 10.1109/TMAG.2021.3060748.
13. M. Fazil and K. R. Rajagopal, "A Novel Air-Gap Profile of Single-Phase Permanent-Magnet Brushless DC Motor for Starting Torque Improvement and Cogging Torque Reduction," in IEEE Transactions on Magnetics, vol. 46, no. 11, pp. 3928-3932, Nov. 2010, doi: 10.1109/TMAG.2010.2057514.
14. Y. -U. Park, J. -H. Cho and D. -k. Kim, "Cogging Torque Reduction of Single-Phase Brushless DC Motor With a Tapered Air-Gap Using Optimizing Notch Size and Position," in IEEE Transactions on Industry Applications, vol. 51, no. 6, pp. 4455-4463, Nov.-Dec. 2015, doi: 10.1109/TIA.2015.2453131.
15. B. -p. Jin, H. Wang, J. -b. Li and Z. -w. Wu, "High Precision Servo Control of Single-phase BLDC motor based on Fuzzy self-tuning PID," 2022 International Symposium on Control Engineering and Robotics (ISCER), Changsha, China, 2022, pp. 38-41, doi: 10.1109/ISCER55570.2022.00013.
16. C. -L. Chiu, Y. -T. Chen and W. -S. Jhang, "Properties of Cogging Torque, Starting Torque, and Electrical Circuits for the Single-Phase Brushless DC Motor," in IEEE Transactions on Magnetics, vol. 44, no. 10, pp. 2317-2323, Oct. 2008, doi: 10.1109/TMAG.2008.2000761.